

1 **Supplementary Material for Research Article in *Climate of the Past*:**
2 **“Orbitally tuned time scale and astronomical forcing in the middle**
3 **Eocene to early Oligocene”**

4 **by T. Westerhold, U. Röhl, H. Pälike, R. Wilkens, P. A. Wilson, G. Acton**

5
6 **Supplementary Document S1: Paleomagnetism of Site U1333**

7 **Introduction**

8 The paleomagnetic data used to determine the magnetostratigraphy for Site U1333
9 (10.51655°N, 221.58072°E, Water Depth 4853 m) are provided as supplementary data tables.
10 This document provides a guide to the data in the tables and additional information about the
11 sampling, measurements, methods, and processing.

12
13 **Background**

14 The sampling strategy, measurement protocol, and magnetostratigraphic interpretation used in
15 the present study was guided by results obtained during Expedition 320 by the shipboard
16 paleomagnetism team (Gary Acton, Yuhji Yamamoto, Christian Ohneiser, Carl Richter, and
17 Helen Evans). Results from that study are available in Pälike et al. (2010), which includes
18 supplementary data tables with paleomagnetic measurements for all archive-half split-core
19 sections and discrete paleomagnetic cube samples (~7 cm³). Vector demagnetization
20 diagrams and principal component analysis (PCA) directions obtained from progressive
21 thermal or alternating field (AF) demagnetization of discrete samples in that study provide
22 constraints on magnetization acquisition and magnetic mineralogy pertinent to this study.

23
24 **Sampling**

25 Three holes (U1333A, B, and C) were cored at Site U1333 in ensure recovery of a complete
26 stratigraphic section. A total of 531.65 m of core was recovered from 49 cores collected using
27 the Advanced Piston Corer (APC) and 17 cores collected using the Extended Core Barrel
28 (XCB) coring system. The XCB cores were not sampled for paleomagnetic analysis in this
29 study because it is not possible to azimuthally reorient the cores, and therefore the
30 paleomagnetic declination is indeterminate. Given the low paleolatitude of Site U1333, the

31 paleomagnetic inclination is also too shallow to confidently determine the magnetic polarity
32 from inclination data along. Thus, we sampled only APC cores.

33 A total of 88 U-channel samples (2 cm x 2 cm x 150 cm) were collected continuously along
34 the spliced composite stratigraphic section from 96 to 190 adjusted revised meters composite
35 depth (rmcd). The stratigraphic splice and rmcd scale are provided in Westerhold et al.
36 (2012).

37

38 **Measurements**

39 Measurements were made in the Paleomagnetism Laboratory at the University of California–
40 Davis using a 2G Enterprises long-core cryogenic magnetometer (Model 755), which resides
41 within a magnetically shielded room. Each U-channel sample was subjected to progressive
42 AF demagnetization from 0 mT up to 80 or 100 mT typically in 8 to 11 steps and the
43 magnetic remanence was measured every 1 cm following each demagnetization step. Raw
44 inclination, declination, and intensity data for each measurement step is provided in
45 Supplementary Tables S17-19.

46

47 **Processing**

48 Paleomagnetic directions were determined from principal component analysis (PCA)
49 (Kirschvink, 1980), in which remanence measurements from at least five demagnetization
50 steps for each interval were fit to lines. Only steps between 20 and 60 mT were used. Program
51 Zplotit (Acton, 2011, <http://paleomag.ucdavis.edu/software-zplotit.html>) was used to search
52 iteratively for the best-fit line segments, determine PCA directions, and produce vector
53 demagnetization diagrams, intensity-decay plots, and stereonet. Lines were fit using both the
54 FREE option of PCA, in which the line is not required to pass through the origin of the plot,
55 and the ANCHORED option of PCA, in which line is anchored to the origin (Supplementary
56 Tables S17-S19). In addition, a Fisherian mean direction was computed from the highest
57 several demagnetization steps used in the PCA. This Fisherian direction is referred to as a
58 stable end point (SEP). Comparison between the FREE PCA, ANCHORED PCA, and SEP
59 can be used to assess the stability of the characteristic remanent magnetization (ChRM) and
60 the presence of unremoved magnetic overprints. The FREE PCA direction is used as the
61 preferred direction in the magnetostratigraphic interpretation.

62 Correlation of the $\sim 180^\circ$ alternations in the composite paleomagnetic declination record with
63 the geomagnetic polarity timescale (GPTS) provides the basis for the magnetostratigraphic
64 interpretation. To construct this record, the declination at the base of the first core collected is
65 matched to the declination from another core from a different hole that contains a coeval
66 interval, and then this process is repeated down the stratigraphic section. This strategy is
67 possible because coring in the three holes is conducted such that there is stratigraphic overlap
68 between cores from the different holes, ensuring that a complete stratigraphic section is
69 obtained. For aesthetic purposes, the declination for each core has been rotated by a constant
70 amount such that the average declination for normal and reversed polarity intervals are
71 approximately 0° and 180° , respectively. Because the Pacific Plate has not rotated much since
72 the Eocene, this also gives declinations that are close to true values. In addition, APC cores
73 sometimes have a small within-core azimuthal rotation, which occurs as the piston corer
74 penetrates the sediments. These tend to produce subtle sigmoidal variations in declination
75 within a core, which are too small to influence the magnetostratigraphic interpretation but that
76 are a bias unrelated to the geomagnetic field. This artifact has been removed by fitting a
77 sigmoid to the declination-vs.-depth data for each core and then subtracting that value from
78 the observed value, in a manner similar to that described by Lanci et al. (2004).

79

80 **Paleomagnetic Results**

81 As shown in Pälike et al. (2010), the Site U1333 sediments are accurate recorders of the
82 paleomagnetic field. Generally, AF demagnetization up to 10 to 20 mT was sufficient to
83 remove drilling-related overprints and resolve the ChRM component in the split-core samples.

84 Our more detailed AF demagnetization results provide confirmation of the stability of the
85 ChRM, while also resolving it more accurately and precisely. Line fits through the
86 demagnetization data using PCA (FREE fitting option) were well constrained, with average
87 maximum angular deviation (MAD) angles of 2.3° for the 10,896 intervals used in the
88 magnetostratigraphic interpretation (Supplementary Figure S12 and Tables S17-S19). The
89 linear decay of magnetization is generally to the origin of the vector demagnetization
90 diagrams, although some samples decay to positions near rather than directly to the origin.
91 We observed that most of those samples that do not decay directly to the origin were from
92 cores that were collected with a standard metal bottom-hole assembly (BHA) and core barrel
93 whereas those samples that decay directly to the origin were collected with a non-magnetic
94 BHA and non-magnetic core barrel. U-channel samples that included more material from the

95 periphery of the core also had stronger drilling overprints. Sampling the core periphery occurs
96 when the split-core section is relatively thin (≤ 2 cm). In either case, the minor overprint does
97 not affect the declinations appreciably and, hence, has no impact on the magnetostratigraphic
98 interpretation.

99 The downhole variation in the ChRM direction is one with fairly consistent shallow
100 inclination, as expected for sediments deposited near the paleo-equator, and with declinations
101 that alternate between two stable states that are antipodal, representing normal and reverse
102 polarity magnetozones (Figure S13). The zonation can readily be correlated to the GPTS, a
103 process that is facilitated by biostratigraphic constraints. Given these properties, it is clear the
104 ChRM is a primary depositional remanent magnetization that records the reversals of the
105 geomagnetic field.

106 Based on the results of AF demagnetization results from the U-channels, thermal
107 demagnetization results conducted on discrete samples during Expedition 320, and a myriad
108 of other rock magnetic measurements conducted on equatorial Pacific sediments from Site
109 U1333 and nearby drill sites (e.g., Lanci et al., 2004 and 2005; Pares and Lanci, 2004; Guidry
110 et al., 2013; Ohneiser et al., 2013; Yamamoto et al., 2013; Yamazaki et al., 2013), the ChRM
111 is carried primarily by biogenic magnetite and detrital titanomagnetite and/or
112 titanomaghemite.

113

114 **Magnetostratigraphic Interpretation**

115 The revised magnetostratigraphy is derived from the distinct $\sim 180^\circ$ alternations in magnetic
116 declination that occur along the composite stratigraphic section (Supplementary Figure S13
117 and Tables S17-S19). Correlation of these with the GPTS illustrates that the magnetozones
118 from 96 to 190 rmdc correspond to chronozones spanning from the middle of Chron C11r to
119 within Chron C20n (Figure S12 and Table 1).

120 This magnetostratigraphic interpretation is basically the same as that given in Pälike et al.
121 (2010), although the locations of the reversals have been refined. The oldest reversal observed
122 by Pälike et al. (2010) was the base of Chron C20n, which occurred near the bottom of the
123 last APC core collected in Hole U1333C. In this study, we interpret only down to the top of
124 Magnetozone C20n. Of the 23 reversals that occur between the base of Magnetozone C11r
125 and top of Magnetozone C20n, the difference between Pälike et al. (2010) and the revised
126 depth estimates is <5 cm for 11 reversals and <20 cm for all but 3 of the remain 12 reversals.
127 The largest change, 163 cm, is for the depth of the reversal associated with the Chron

128 C12r/C13n boundary. For Hole U1333C, this could only be constrained to occur between
129 Cores U1333C-13H and -14H in the split-core data but could be constrained to occur at about
130 47 cm from the top of Core U1333C-14H in the U-channel data.

131

132 **Ages**

133 We use the ages from the astronomically tuned age model for Site U1333 from this paper
134 (Supplementary Table S15). The age model encompasses all sediments deposited from the
135 base of Chron C12n to the top of Chron C20n. The paleomagnetic data extend through that
136 entire interval and a few meters up section through sediments that were deposited during
137 Chron C11r. For these younger sediments, we use the ages from Pälike et al. (2006).

138

139 **Paleomagnetic Data Tables**

140 The following is a description of the paleomagnetic data provided in Tables S17-S19:

141 **U-channel Sample:** The naming convention follows that from IODP. For example, sample
142 U1333A-10H-1 is a U-channel collected along Section 1 of Core 10H from Hole U1333A.

143

144 **Interval:** The interval along the U-channel measured from the top.

145

146 **Depths:**

147 mbsf = meters below seafloor = CSF-A

148 mcd = meters composite depth = CCSF-A

149 amcd = adjusted mcd = rmc = revised adjusted CCSF-A

150

151 **Age:** The ages are from this paper for the interval from Chron C12n (o) to C20n (y). Ages
152 from Pälike et al. (2010) are used for younger chrons.

153

154 **Half:** Working (W) or Archive (A) half of the split-core sections.

155

156 **Filter 1:** This column is for culling data. It contains a 0 if the interval is considered biased or
157 a 1 if the data are considered valid. Data are considered biased if they fall within disturbed
158 intervals identified during sampling or based on core descriptions made on Expedition 320
159 (Pälike et al., 2010)

160

161 **Filter 2:** This column is for further culling data. Filter 2 is like Filter 1, but it also eliminates
162 data within 4 cm of the ends of the U-channel samples, which often are biased by sample edge
163 effects. This filter was used for the data in the magnetostratigraphic interpretation.

164

165 **Raw Data:** Columns with the prefix AFD, Dec, Inc, and Int followed by three numbers are
166 the AF demagnetization step (mT), declination, inclination, and intensity (A/m). The three
167 numbers give the demagnetization step. Hence AFD030, Dec030, Inc030, and Int030 are the
168 data for the 30 mT demagnetization step.

169

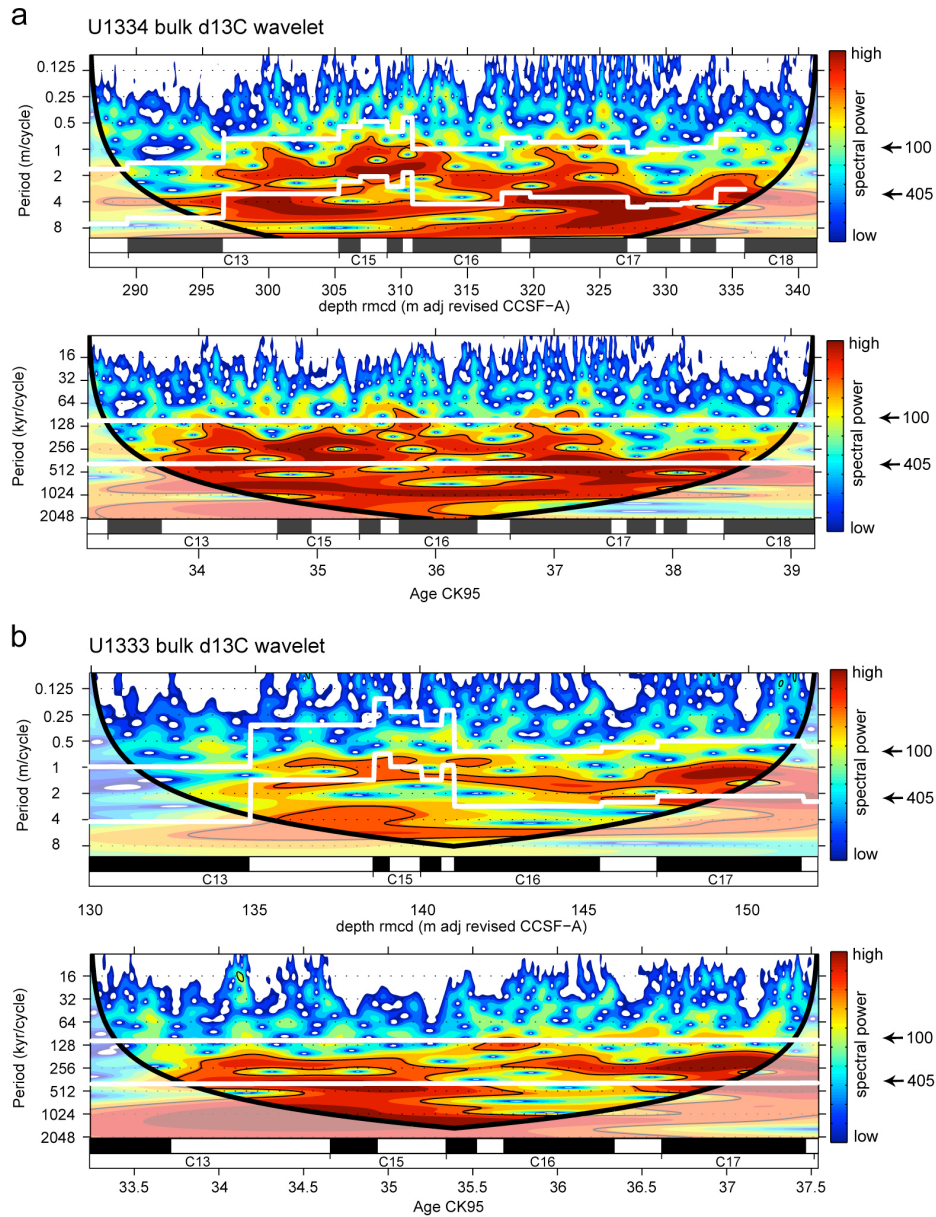
170 **PCA:** Principal component analysis for FREE and ANCHORED lines, from program Zplotit
171 (Acton, 2011, <http://paleomag.ucdavis.edu/software-zplotit.html>).
172

173 **Declination Corrected for Constant & Within-Core Rotation:** The preferred declination,
174 which is the declination determined from the FREE PCA option corrected for azimuthal
175 rotation of the core and for minor within core rotation as described above.
176

177 **Polarity:** N for normal, R for reversed, and X for disturbed or indeterminate intervals.
178

179 **Chron:** The polarity chron name. An X is put in the column for disturbed intervals.
180

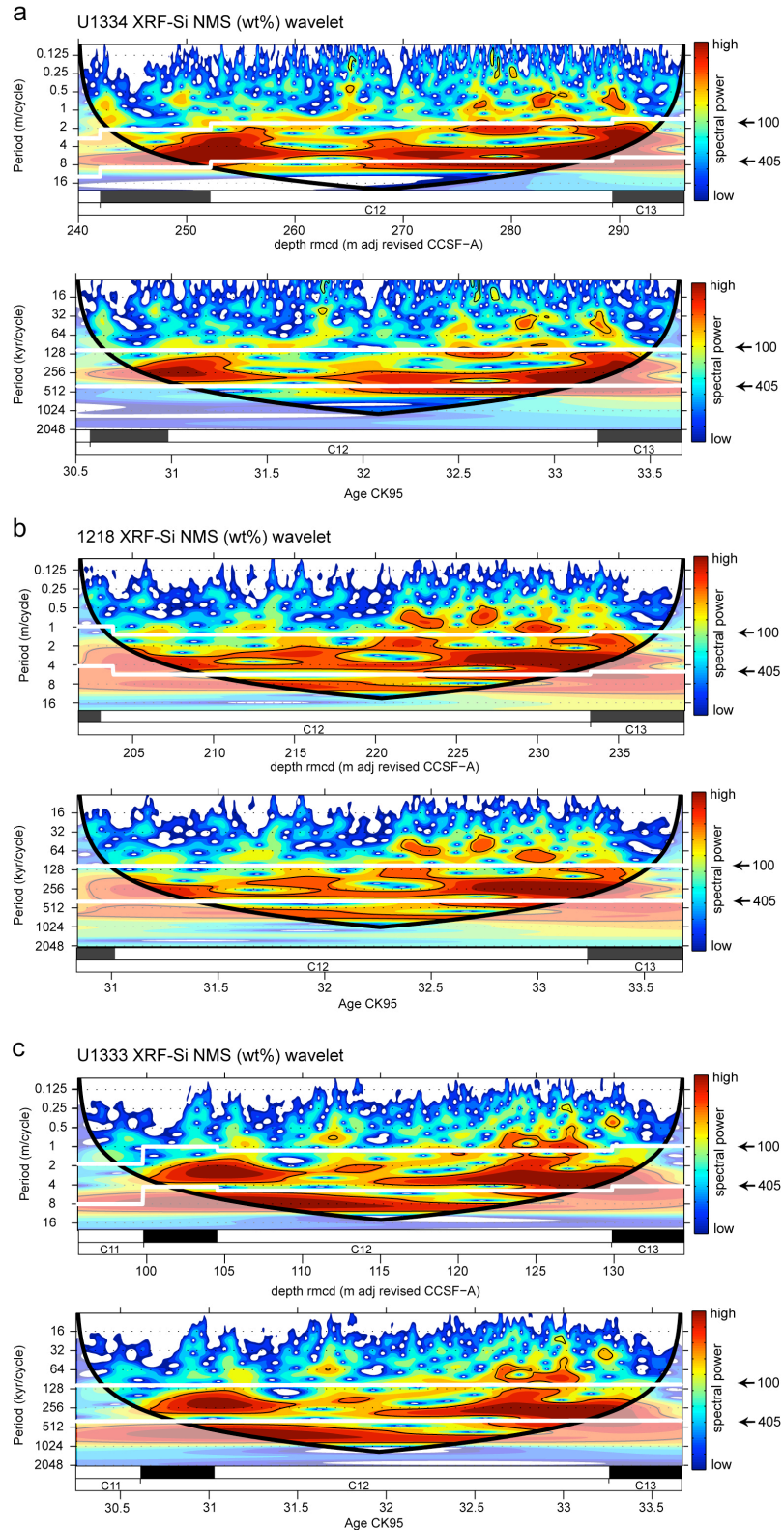
181 **Supplementary Material - Figures**



182

183 Figure S1. Evolutionary wavelet power spectra of bulk stable carbon isotope data from
 184 Site U1334 (a) and U1333 (b) for magnetochrons C13 to C18n.1n in the depth domain and
 185 versus age. The age model is based on magnetostratigraphy using the Time Scale of Cande
 186 and Kent (1995, CK95). The shaded contours in the evolutionary wavelet power spectra are
 187 normalized linear variances with blue representing low spectral power, and red representing
 188 high spectral power. The black contour lines enclose regions with more than 95% confidence.
 189 Shaded regions on either end indicate the cone of influence where edge effects become
 190 important. Distinct bands that run across the spectra indicate the dominance of Milankovitch
 191 frequencies. Thick white lines are the projected 100 and 405-kyr cycle path, respectively.

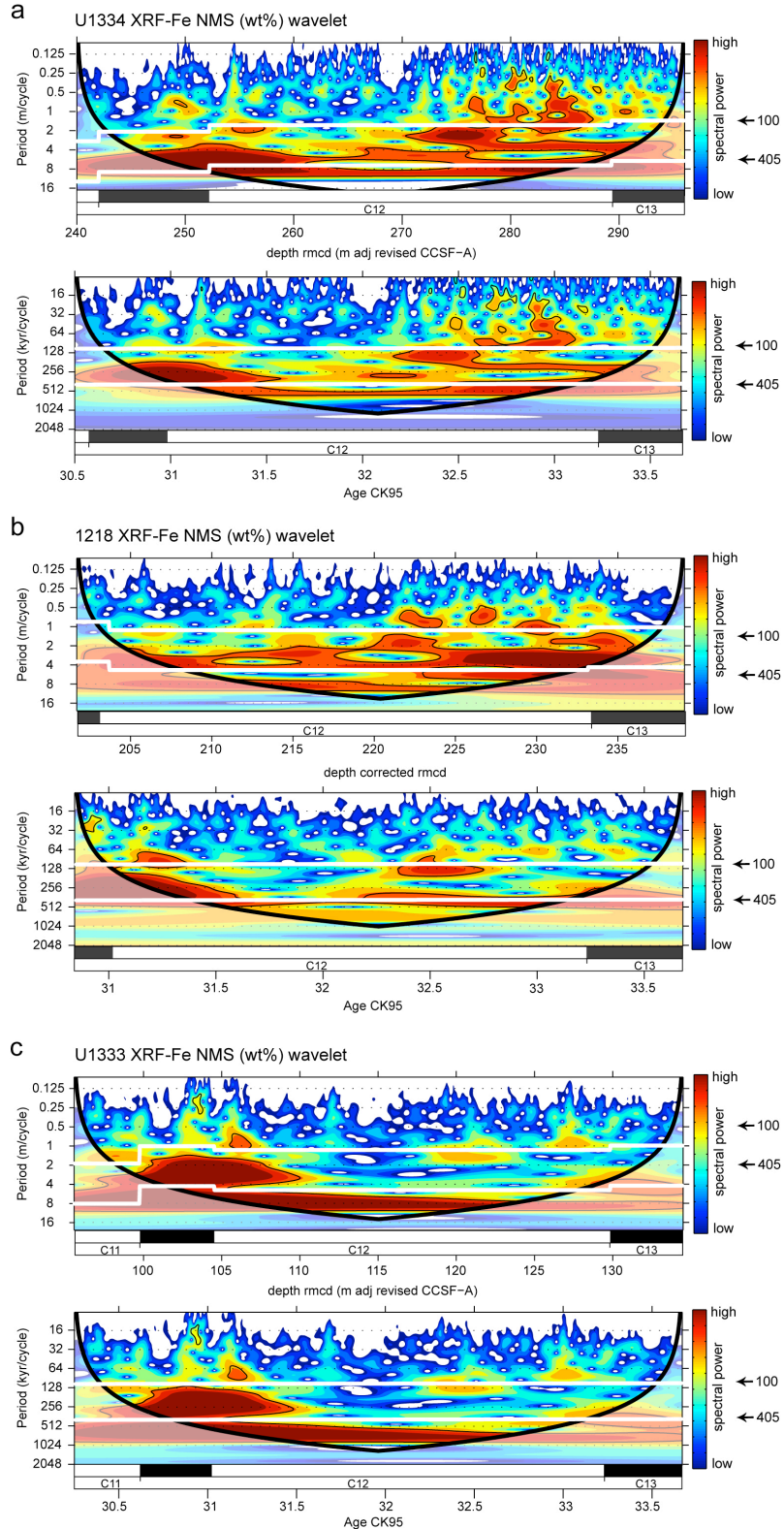
192



193

194 Figure S2. Evolutionary wavelet power spectra of XRF core scanning Normalized Median
 195 Scaled (NMS) Si intensity data expressed as SiO_2 wt% data from Site U1334 (a), 1218 (b) and
 196 U1333 (c) for the Oligocene magnetochrons C12n to C13n in the depth domain and versus
 197 age. For further explanation see Figure S1 text.

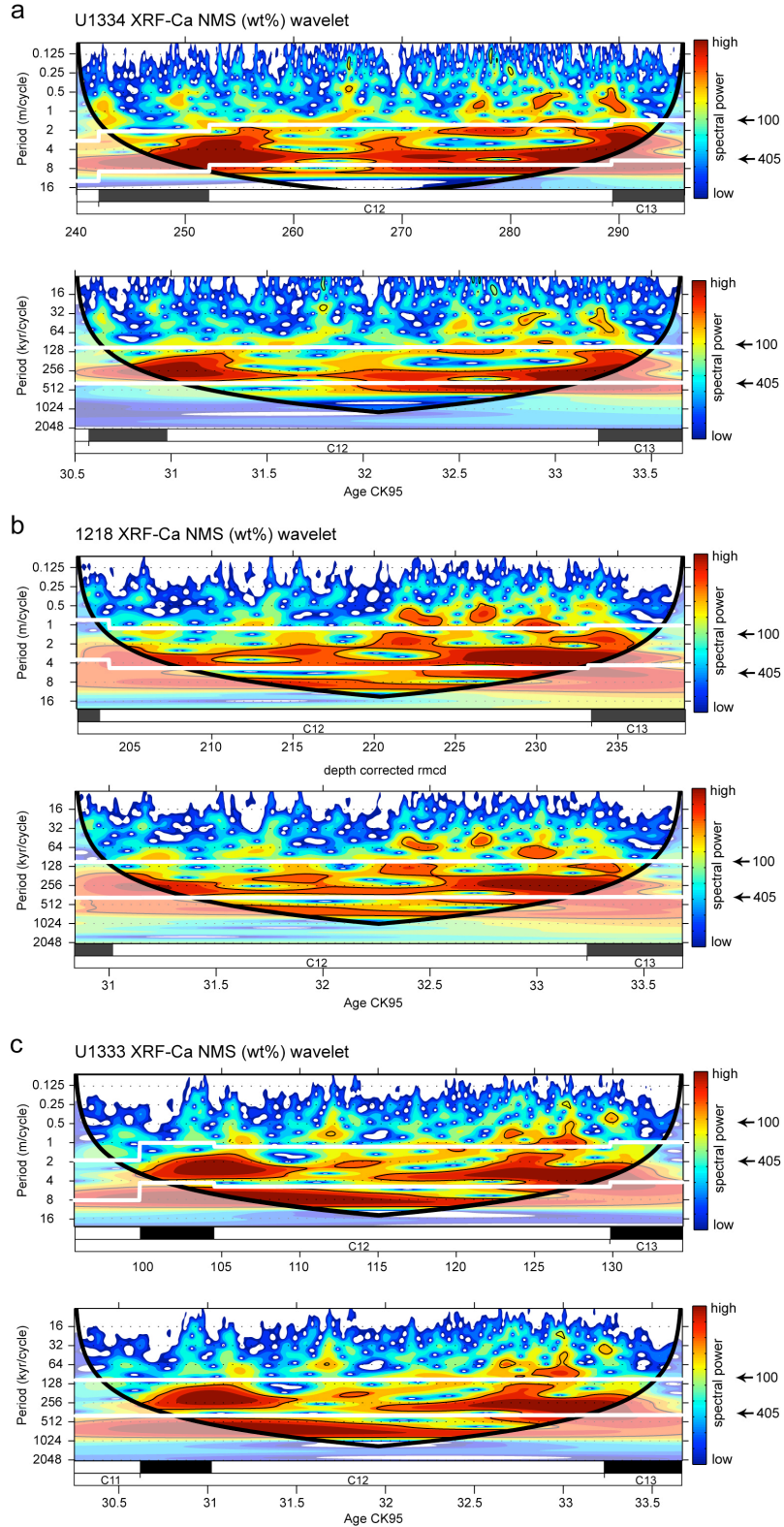
198



199

200 Figure S3. Evolutionary wavelet power spectra of XRF core scanning Normalized Median
 201 Scaled (NMS) Fe intensity data expressed as Fe_2O_3 wt% data from Site U1334 (a), 1218 (b)
 202 and U1333 (c) for the Oligocene magnetochrons C12n to C13n in the depth domain and
 203 versus age. For further explanation see Figure S1 text.

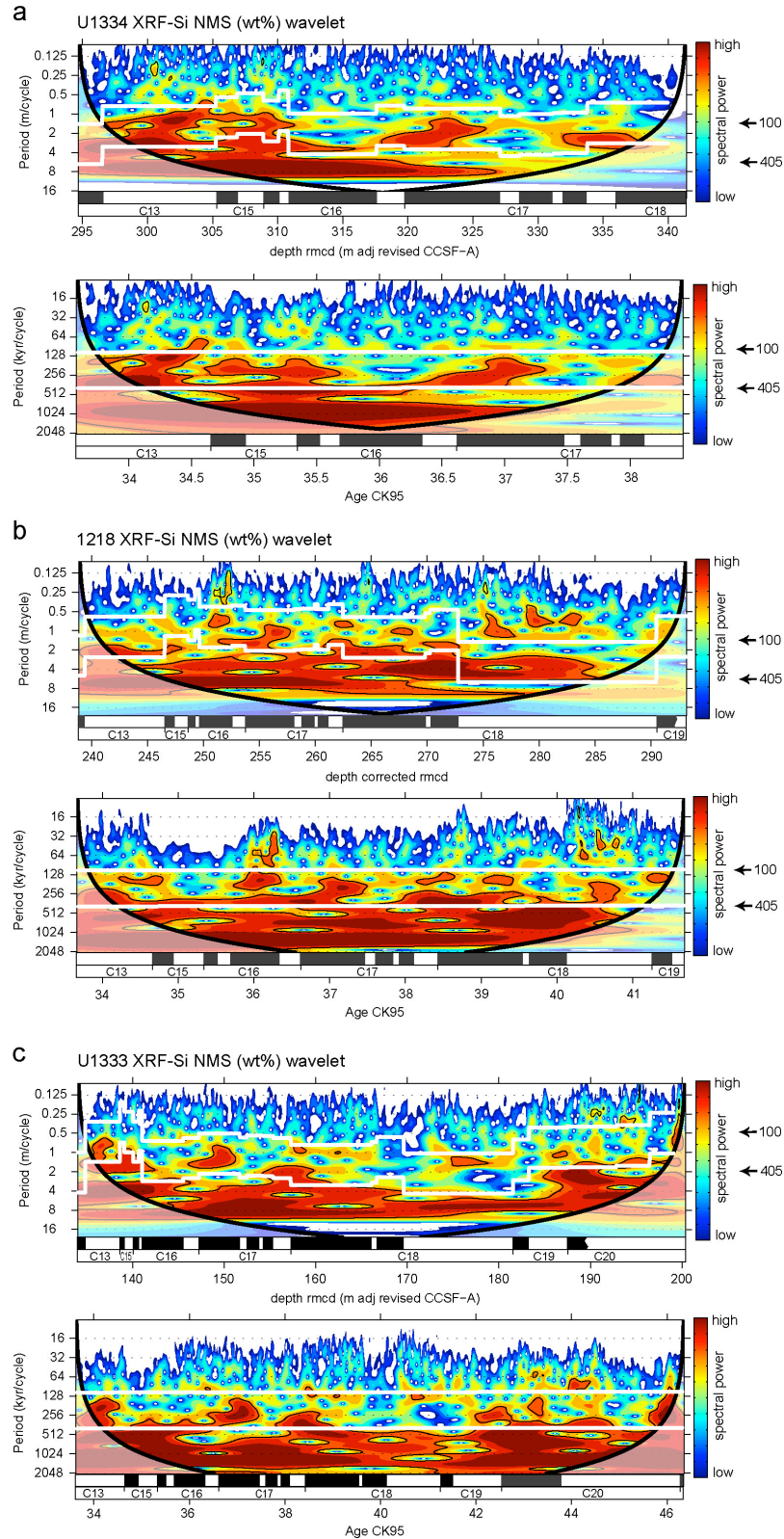
204



205

206 Figure S4. Evolutionary wavelet power spectra of XRF core scanning Normalized Median
 207 Scaled (NMS) Ca intensity data expressed as CaCO_3 wt% from Site U1334 (a), 1218 (b) and
 208 U1333 (c) for the Oligocene magnetochrons C12n to C13n in the depth domain and versus
 209 age. For further explanation see Figure S1 text.

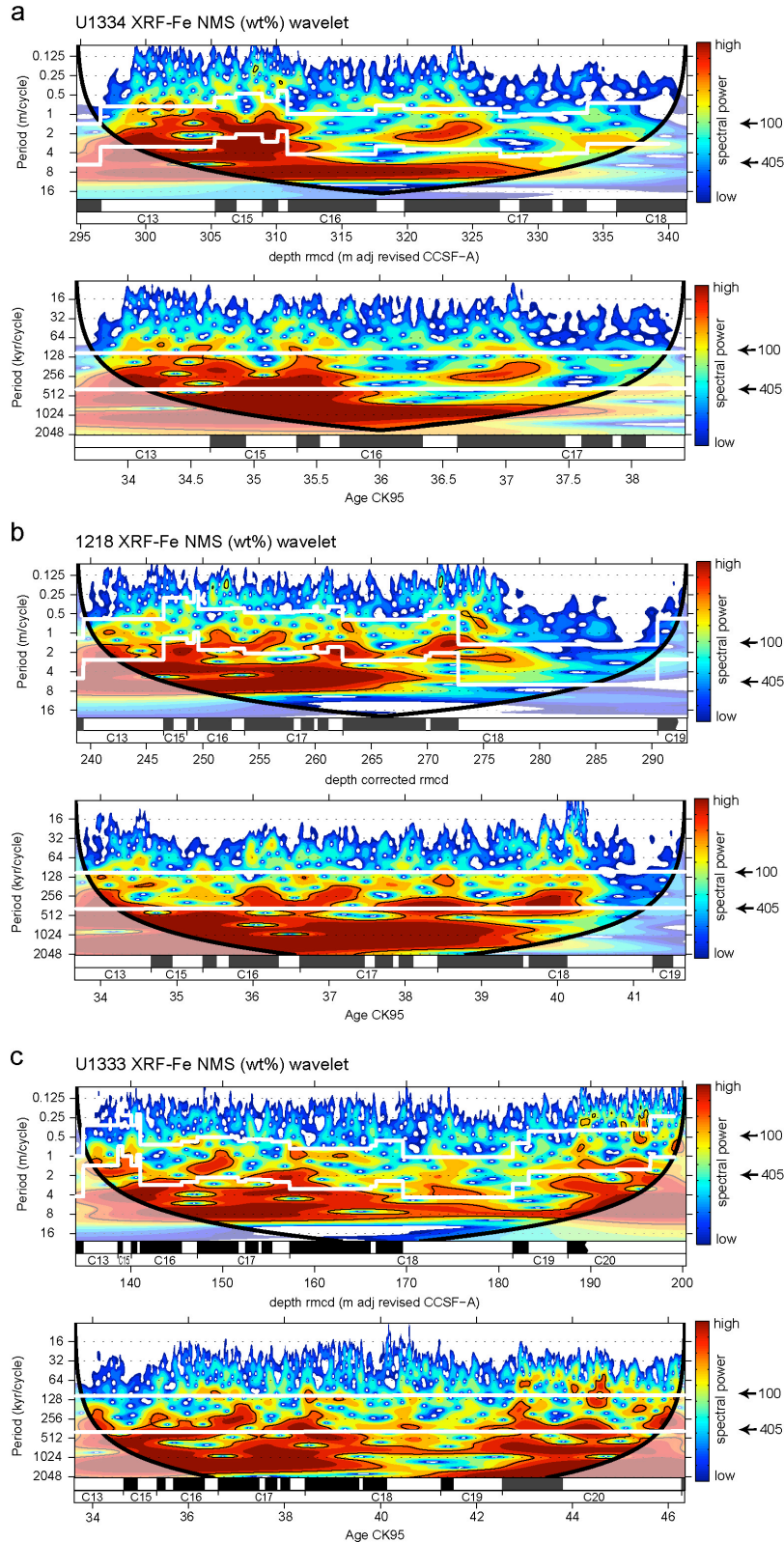
210



211

212 Figure S5. Evolutionary wavelet power spectra of XRF core scanning Normalized Median
 213 Scaled (NMS) Si intensity data expressed as SiO₂ wt% data from Site U1334 (a), 1218 (b) and
 214 U1333 (c) for the Eocene magnetochrons C13r to C20r in the depth domain and versus age.
 215 For further explanation see Figure S1 text.

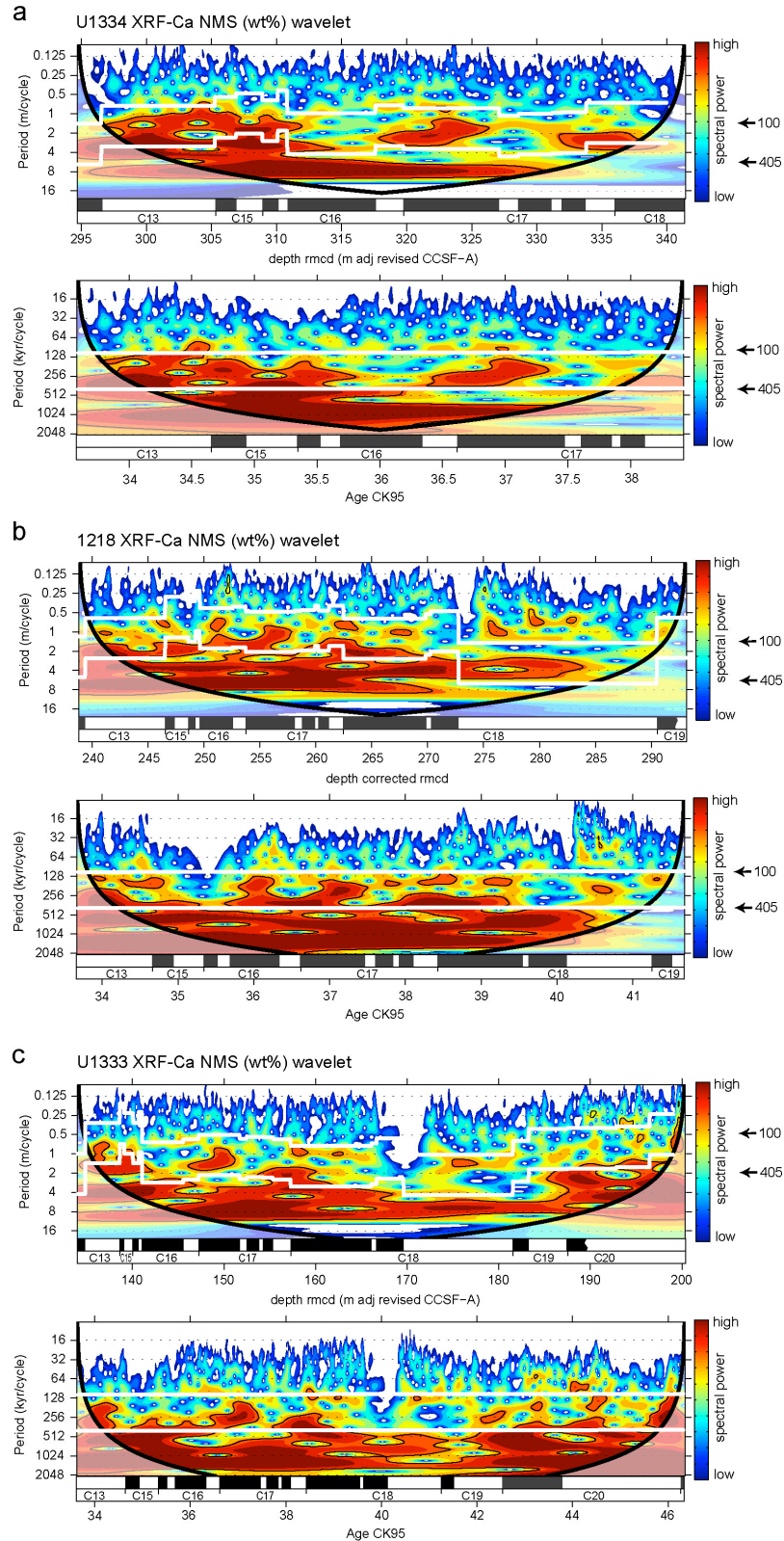
216



217

218 Figure S6. Evolutionary wavelet power spectra of XRF core scanning Normalized Median
 219 Scaled (NMS) Fe intensity data expressed as Fe₂O₃ wt% data from Site U1334 (a), 1218 (b)
 220 and U1333 (c) for the Eocene magnetochrons C13r to C20r in the depth domain and versus
 221 age. For further explanation see Figure S1 text.

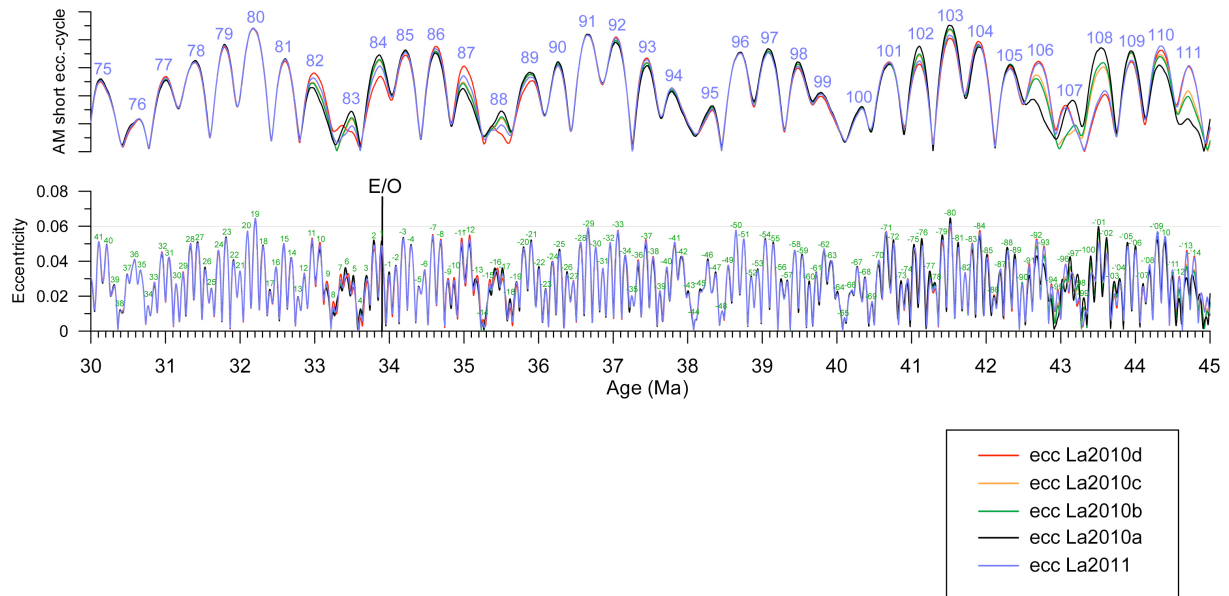
222



223

224 Figure S7. Evolutionary wavelet power spectra of XRF core scanning Normalized Median
 225 Scaled (NMS) Ca intensity data expressed as CaCO₃ wt% from Site U1334 (a), 1218 (b) and
 226 U1333 (c) for the Eocene magnetochrons C13r to C20r in the depth domain and versus age.
 227 For further explanation see Figure S1 text.

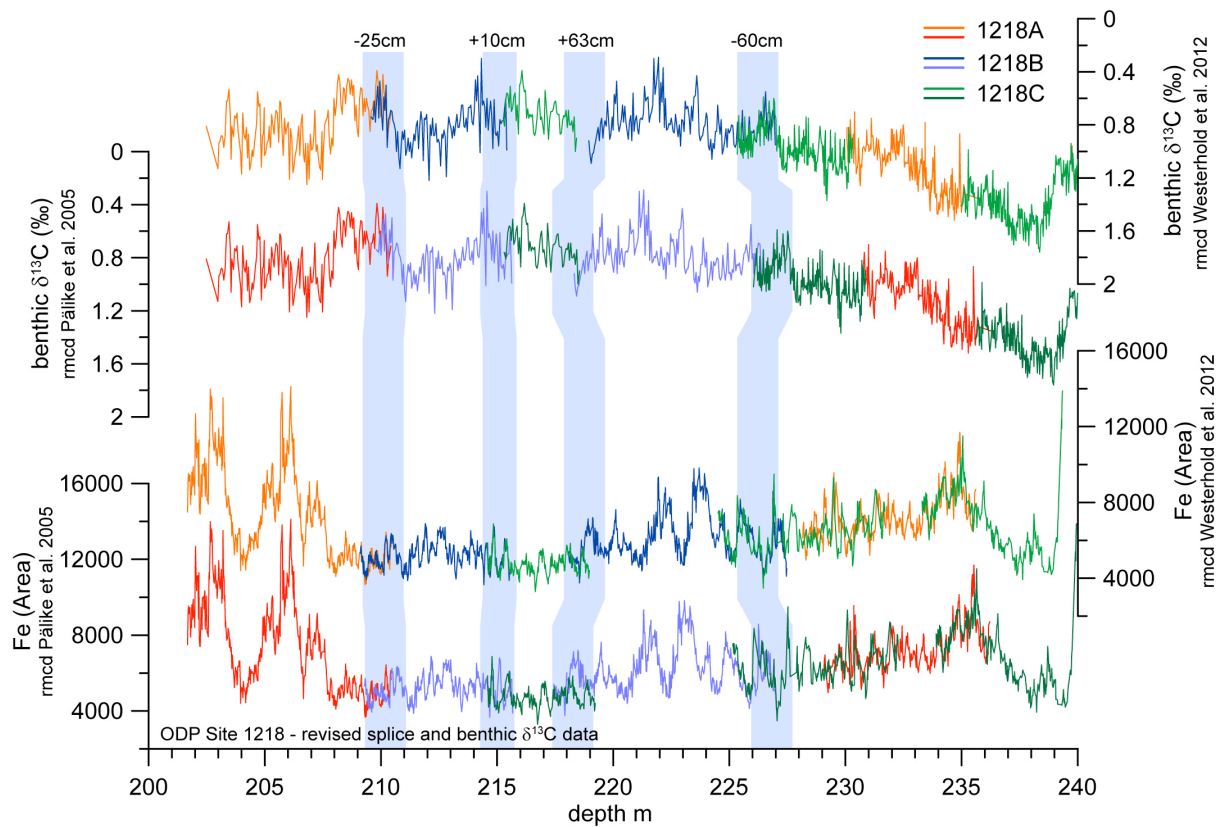
228



229

230 Figure S8. Short (100 kyr) and long (405 kyr) eccentricity cycle number definition for the
 231 astronomical solutions from 30 to 45 Ma as used in this publication. Lower panel shows
 232 earth's orbital solution for eccentricity from Laskar et al. (2011a, four solutions a to d) and
 233 Laskar et al. (2011b). Each short eccentricity is labeled with a number (green) counting from
 234 the in this paper established position of the Eocene/Oligocene boundary. This facilitates
 235 comparing the cycle extracted from the geological data to the orbital solution. The upper
 236 panel shows the amplitude modulations extracted with the program ENVELOPE (Schulz et
 237 al., 1999) of the short eccentricity cycle. For details about the solutions and their stability over
 238 time see the discussion in Westerhold et al. (2012b).

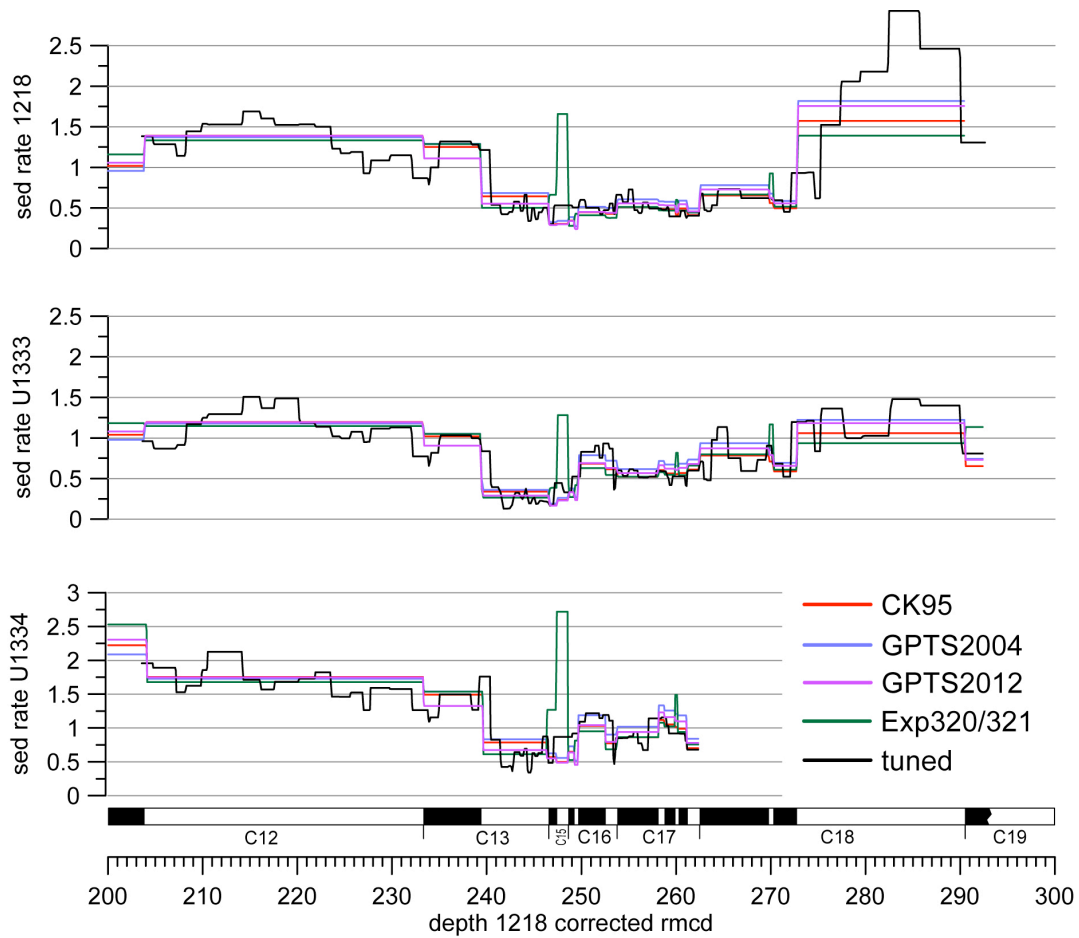
239



240

241 Figure S9. XRF core scanning Fe (Iron) intensity data (this study) and benthic $\delta^{13}\text{C}$ data
 242 from ODP Site 1218 (Coxall et al., 2005; Wade and Pälke, 2004; Pälke et al., 2006; Coxall
 243 and Wilson, 2011) plotted on the rmcd of Pälke et al. (2005) and the corrected rmcd of
 244 Westerhold et al. (2012a) to illustrate changes in the composite record. Data are plotted for
 245 holes 1218A (red), 1218B (blue) and 1218C (green) separately to highlight overlaps, gaps and
 246 mismatches. The blue bars mark changes in the composite record including the amount of
 247 change in cm. As an example, the change around 227 m illustrates that the splice of Pälke et
 248 al. (2005) doubled a prominent $\delta^{13}\text{C}$ decrease (one full 100-kyr eccentricity cycle) and
 249 therefore retuning of this interval was required.

250

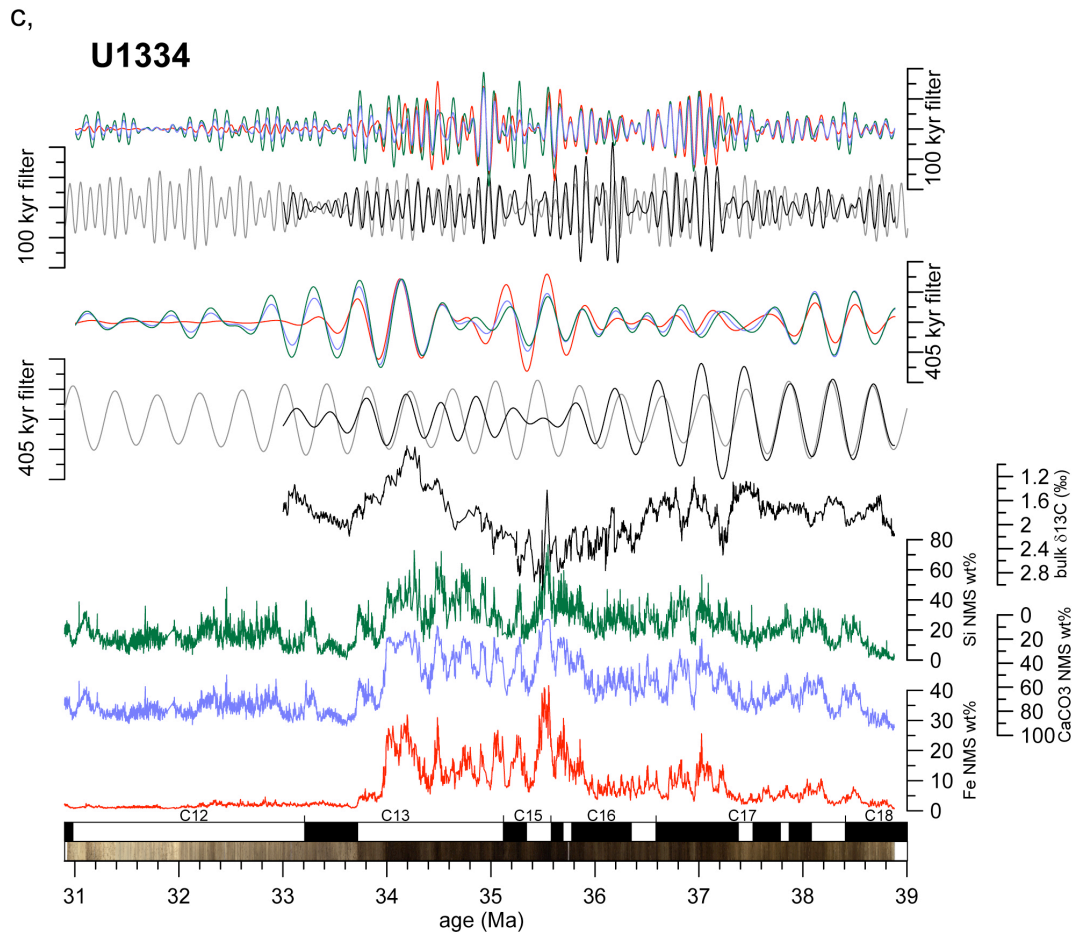


251

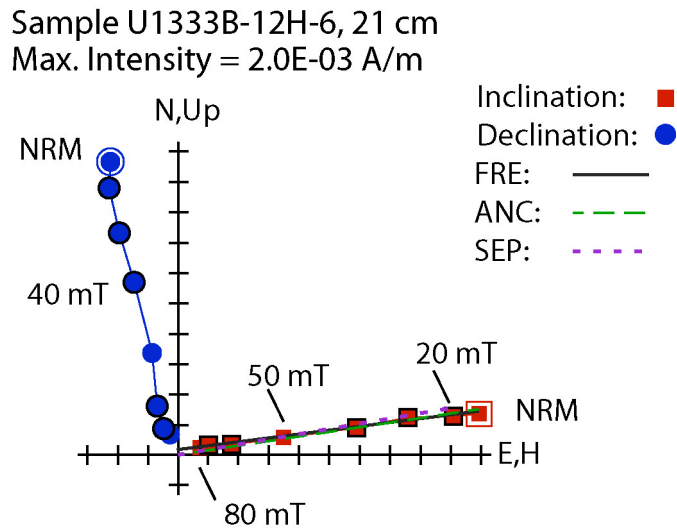
252 Figure S10. Sedimentation rate plots for Sites 1218, U1333 and U1334 based on
 253 magnetostratigraphy and different ages for magnetostratigraphic boundaries mapped onto 1218
 254 corrected rmc. CK95 - Cande and Kent 1995; GPTS2004 – Geomagnetic Polarity Time
 255 Scale 2004 - Ogg and Smith (2004); GPTS2012 – Ogg (2012); Exp320/321 – Pälike et al.
 256 (2010) based on Pälike et al. (2006); tuned – this paper.

257

259 Figure S11 a & b. Calibrated XRF Fe (red), Ca (blue), and Si (green) core scanning data,
 260 stable isotope data (black) and band pass filters plotted on the tuned age model for sites 1218
 261 (a) and U1333 (b). Grey curve is the 100 (0.1 ± 0.03 cycles/kyr) and 405 (0.02469 ± 0.007)
 262 kyr filter of the La2011 (Laskar et al. 2011) orbital solution. Filters for data are only given at
 263 intervals where the resolution is high enough to resolve the cyclicity.
 264



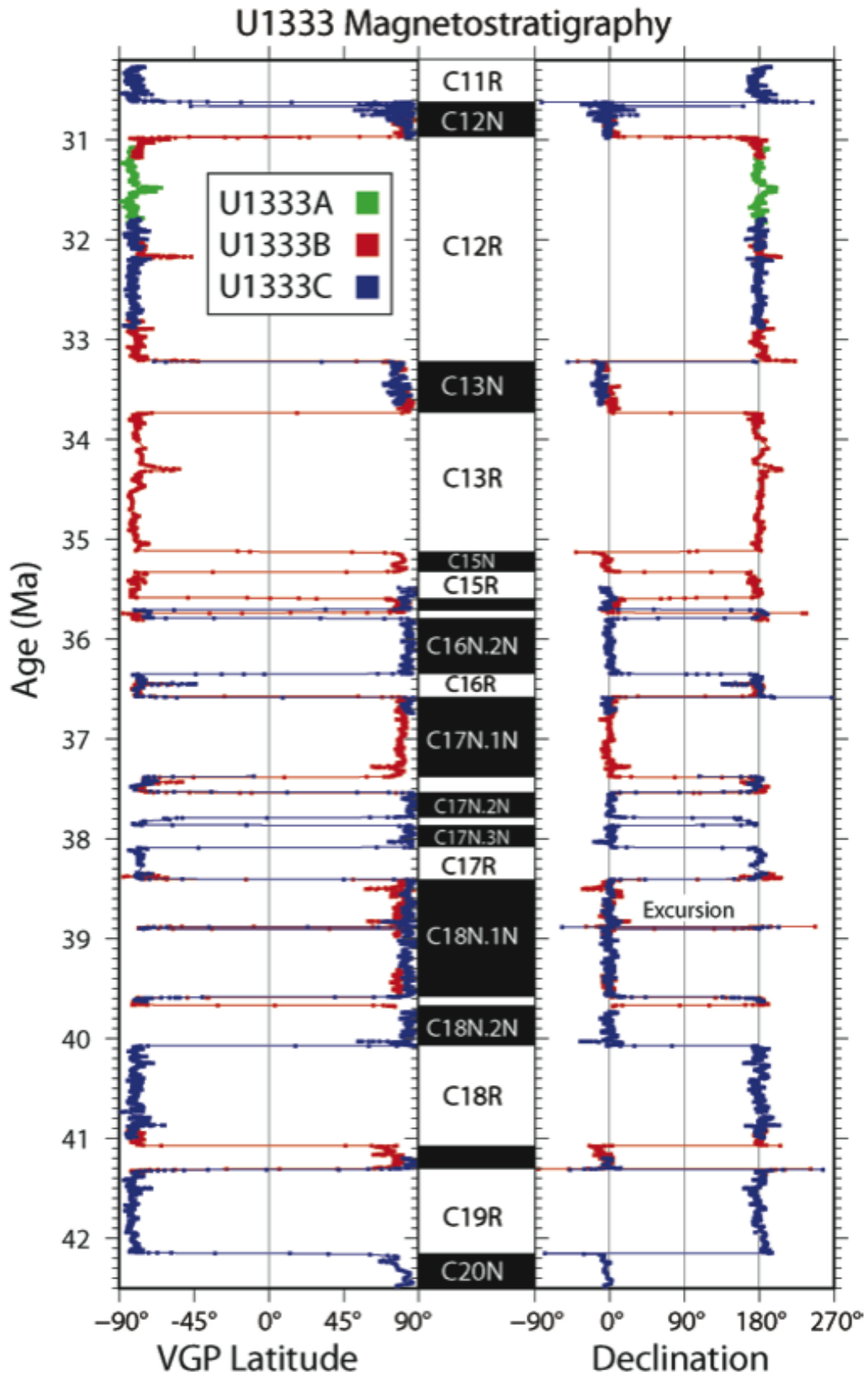
265
 266 Figure S11 c. Calibrated XRF core scanning data, stable isotope data and band pass filters
 267 plotted on the tuned age model for Site U1334. For further reference see Fig. S11a&b.
 268



269

270 Figure S12. A typical vector demagnetization diagram for an interval along a U-channel
 271 sample. This particular U-channel was taken from an archive half core, which had been AF
 272 demagnetized at 20 mT during Expedition 320. That was sufficient to remove the low-
 273 coercivity drilling overprint common to IODP cores. The remaining magnetization decays to
 274 the origin illustrating the univectorial nature of the remanent magnetization. Lines fit through
 275 the data (shown only for the inclination) using the FREE and ANCHORED options of PCA
 276 and a Fisherian mean (SEP) are so similar that they plot on top of each other.

277



278

279 Figure S13. Magnetostratigraphy of Site U1333 from U-channel paleomagnetic data. The
 280 virtual geomagnetic pole (VGP) latitude and the declination are plotted versus age.

281

282 **Supplementary Material - Tables**

283 The complete data set presented is available online in the WDC-MARE PANGAEA database
284 at <http://doi.pangaea.de/10.1594/PANGAEA.821903>

285

286 Table S1. ODP Site 1218 XRF splice data

287 Table S2. ODP Site 1218A XRF raw data

288 Table S3. ODP Site 1218B XRF raw data

289 Table S4. ODP Site 1218C XRF raw data

290 Table S5. IODP Site U1333 XRF splice data

291 Table S6. IODP Site U1333A XRF raw data

292 Table S7. IODP Site U1333B XRF raw data

293 Table S8. IODP Site U1333C XRF raw data

294 Table S8. IODP Site U1334 XRF splice data

295 Table S10. IODP Site U1334A XRF raw data

296 Table S11. IODP Site U1334B XRF raw data

297 Table S12. IODP Site U1334C XRF raw data

298 Table S13. IODP Site U1333 bulk stable carbon isotope data

299 Table S14. IODP Site U1334 bulk stable carbon isotope data

300 Table S15. Astronomical tuned age model for Sites 1052, 1218, U1333 and U1334.

301 Table S16. Magnetostratigraphy and astronomically tuned ages of magnetochron
302 boundaries of Sites 1218, U1333 and U1334.

303 Table S17. U1333A U-channel paleomagnetic data

304 Table S18. U1333B U-channel paleomagnetic data

305 Table S19. U1333C U-channel paleomagnetic data

306

307 **References in supplementary**

- 308 Cande, S. C., and Kent, D. V.: Revised calibration of the geomagnetic polarity timescale for the Late Cretaceous
309 and Cenozoic, *Journal of Geophysical Research*, 100, 6093-6095, 1995.
- 310 Coxall, H. K., Wilson, P. A., Pälike, H., Lear, C. H., and Backman, J.: Rapid stepwise onset of Antarctic
311 glaciation and deeper calcite compensation in the Pacific Ocean, *Nature*, 433, 53-57, 10.1038/nature03135,
312 2005.
- 313 Coxall, H. K., and Wilson, P. A.: Early Oligocene glaciation and productivity in the eastern equatorial Pacific:
314 Insights into global carbon cycling, *Paleoceanography*, 26, PA2221, 10.1029/2010pa002021, 2011.
- 315 Guidry, E. P., Richter, C., Acton, G. D., Channell, J. E. T., Evans, H. F., Ohneiser, C., Yamamoto, Y., and
316 Yamazaki, T., 2013. Oligocene-Miocene magnetostratigraphy of deep-sea sediments from the Equatorial
317 Pacific (IODP Site U1333), *Geol. Soc. London, Spec. Pub.*, 373, 13-27, doi:10.1144/SP373.7.
- 318 Lanci, L., Pares, J.M., Channell, J.E.T., and Kent, D.V., 2004. Miocene magnetostratigraphy from Equatorial
319 Pacific sediments (ODP Site 1218, Leg 199). *Earth Planet. Sci. Lett.*, 226, 207-224.
- 320 Lanci, L., ParÈs, J.M., Channell, J.E.T., and Kent, D.V., 2005. Oligocene magnetostratigraphy from Equatorial
321 Pacific sediments (ODP Sites 1218 and 1219, Leg 199). *Earth Planet. Sci. Lett.*, 237, 617-634.
- 322 Laskar, J., Robutel, P., Joutel, F., Gastineau, M., Correia, A., and Levrard, B.: A long-term numerical solution
323 for the insolation quantities of the Earth, *Astronomy and Astrophysics*, 428, 261-285, 10.1051/0004-
324 6361:20041335, 2004.
- 325 Laskar, J., Fienga, A., Gastineau, M., and Manche, H.: La2010: a new orbital solution for the long-term motion
326 of the Earth, *Astronomy and Astrophysics*, 532, A89, 10.1051/0004-6361/201116836, 2011a.
- 327 Laskar, J., Gastineau, M., Delisle, J. B., Farrès, A., and Fienga, A.: Strong chaos induced by close encounters
328 with Ceres and Vesta, *Astronomy and Astrophysics*, 532, L4, 10.1051/0004-6361/201117504, 2011b.
- 329 Ogg, J. G., and Smith, A. G.: The geomagnetic polarity time scale, in: *A Geological Timescale 2004*, edited by:
330 Gradstein, F., Ogg, J., and Smith, A., Cambridge University Press, 63-86, 2004.
- 331 Ogg, J. G.: Geomagnetic Polarity Time Scale, in: *The Geological Timescale 2012*, edited by: Gradstein, F., Ogg,
332 J., Schmitz, M. D., and Ogg, G. M., Elsevier, 85-114, 2012.
- 333 Ohneiser, C., Acton, G., Channell, J.E.T., Wilson, G.S., Yamamoto, Y., and Yamazaki, T., 2013. A middle
334 Miocene relative geomagnetic paleointensity record from the equatorial Pacific, *Earth Planet. Sci. Lett.*, 374,
335 227-238, doi: dx.doi.org/10.1016/j.epsl.2013.04.038
- 336 Pälike, H., Moore, T., Backman, J., Raffi, I., Lanci, L., Parès, J. M., and Janecek, T.: Integrated stratigraphic
337 correlation and improved composite depth scales for ODP Sites 1218 and 1219, in: *Proc. ODP, Sci. Results,*
338 199: College Station, TX (Ocean Drilling Program), edited by: Wilson, P. A., Lyle, M., and Firth, J. V., 1-41,
339 10.2973/odp.proc.sr.199.213.2005, 2005.
- 340 Pälike, H., Norris, R. D., Herrle, J. O., Wilson, P. A., Coxall, H. K., Lear, C. H., Shackleton, N. J., Tripathi, A. K.,
341 and Wade, B. S.: The Heartbeat of the Oligocene Climate System, *Science*, 314, 1894-1898,
342 10.1126/science.1133822, 2006.
- 343 Pälike, H., Nishi, H., Lyle, M., Raffi, I., Gamage, K., Klaus, A., and the Expedition 320/321 Scientists: *Proc.*
344 *IODP, 320/321: Tokyo (Integrated Ocean Drilling Program Management International, Inc.)*, 2010.
- 345 Pares, J.M., and Lanci, L., 2004. A Middle Eocene – Early Eocene magnetic polarity stratigraphy in equatorial
346 Pacific sediments. In: J.E.T. Channell, D.V. Kent, W. Lowrie, and J.G. Meert (Editors), *Timescales of the*
347 *Paleomagnetic Field*. Amer. Geophysical Union, Washington DC, pp. 131-140.
- 348 Schulz, M., Berger, W. H., Sarnthein, M., and Grootes, P. M.: Amplitude variations of 1470-year climate
349 oscillations during the last 100,000 years linked to fluctuations of continental ice mass, *Geophysical*
350 *Research Letters*, 26, 3385-3388, 1999.
- 351 Wade, B. S., and Pälike, H.: Oligocene climate dynamics, *Paleoceanography*, 19, PA4019,
352 10.1029/2004PA001042, 2004.
- 353 Westerhold, T., Röhl, U., Wilkens, R., Pälike, H., Lyle, M., Jones, T. D., Bown, P., Moore, T., Kamikuri, S.,
354 Acton, G., Ohneiser, C., Yamamoto, Y., Richter, C., Fitch, P., Scher, H., Liebrand, D., and the Expedition
355 320/321 Scientists: Revised composite depth scales and integration of IODP Sites U1331-U1334 and ODP
356 Sites 1218-1220, in: *Proc. IODP, 320/321: Tokyo (Integrated Ocean Drilling Program Management*

- 357 International, Inc.), edited by: Pälike, H., Lyle, M., Nishi, H., Raffi, I., Gamage, K., Klaus, A., and the
358 Expedition 320/321 Scientists, 10.2204/iodp.proc.320321.201.2012, 2012a.
- 359 Westerhold, T., Röhl, U., and Laskar, J.: Time scale controversy: Accurate orbital calibration of the early
360 Paleogene, *Geochem. Geophys. Geosyst.*, 13, Q06015, 10.1029/2012gc004096, 2012b.
- 361 Yamamoto, Y., Yamazaki, T., Acton, G., Richter, C., Guidry, E.P., and Ohneiser, C., 2013. Palaeomagnetic
362 study of IODP Sites U1331 and U1332 in the equatorial Pacific—extending relative geomagnetic
363 palaeointensity observations through the Oligocene and into the Eocene, *Geophys. J. Int.*, doi:
364 10.1093/gji/ggt412.
- 365 Yamazaki, T., Yamamoto, Y., Acton, G., Guidry, E.P., and Richter, C., 2013. Rock-magnetic artifacts on long-
366 term relative paleointensity changes in sediments, *Geochem. Geophys. Geosyst.*, 14, 1-15,
367 doi:10.1029/2012GC004546